Rare Metal Materials and Engineering
Volume 52, Issue 11, November 2023
Available online at www.rmme.ac.cn

Science Press

Cite this article as: Sha Minghong, Wang Shuang, Li Shengli, et al. Effect of Mo on Microstructure and Properties of AlCoCrFeNiMo$_x$ High Entropy Alloy Coatings Prepared by Laser Cladding[J]. Rare Metal Materials and Engineering, 2023, 52(11): 3685-3690. DOI: 10.12442/j.issn.1002-185X.E20230007.

ARTICLE

Effect of Mo on Microstructure and Properties of AlCoCrFeNiMo$_x$ High Entropy Alloy Coatings Prepared by Laser Cladding

Sha Minghong[1,2], Wang Shuang[2,3], Li Shengli[1], Jia Chuntang[2,3], Huang Tiandang[1], Zhu Xiaolei[2,3], Ai Xingang[1], Liao Xiangwei[2,3]

[1] School of Materials and Metallurgy, University of Science and Technology LiaoNing, Anshan 114051, China; [2] State Key Laboratory of Metal Material for Marine Equipment and Application, Anshan 114009, China; [3] Steel Research Institute, Angang Group, Anshan 114009, China

Abstract: AlCoCrFeNiMo$_x$ (x=0, 0.5, 1.0, 1.5, 2.0) high entropy alloy (HEA) coatings were prepared by laser cladding method. The effect of Mo content on the microstructure, hardness, and corrosion resistance of the coatings was studied. Results show that with increasing the Mo content, the microstructure is changed from (Al, Ni)-rich body-centered cubic (bcc) phase+(Mo-Cr-Fe)-rich σ phase into (Fe, Ni)-rich bcc phase+(Mo-Cr-Fe)-rich σ phase+(Al-Fe-Mo)-rich σ phase+a little AlN (aluminum nitride). Additionally, the coating hardness (HV_1) is increased from 6514.4 MPa to 10652.6 MPa. With increasing the Mo addition, the self-corrosion potential of the coating in 3.5wt% NaCl solution is also increased. The coating presents the optimal corrosion resistance at x=1.0.

Key words: HEA; laser cladding; corrosion resistance; hardness; microstructure

High entropy alloys (HEAs) are initially defined as the alloys with high configuration entropy in a regular liquid state[1–2]. HEAs tend to form simple solid solution structures, such as face-centered cubic (fcc) phase, body-centered cubic (bcc) phase, or close-packed hexagonal (hcp) phase, owing to the influence of high configuration entropy. Besides, intermetallic compounds may exist in some HEAs[3–6]. HEAs possess the characteristics of high strength, good phase stability, fine wear resistance, and excellent corrosion resistance because of their special composition and structures[7–9]. The phase structure of AlCoCrFeNi HEAs is usually affected by the element content and heat treatment process. It is reported that Co and Ni are beneficial to form fcc phase and Al is beneficial to form bcc and b2 phases[10–13]. Mo has high temperature strength, high hardness, and strong corrosion resistance[14–15]. It is discussed that the Mo addition promotes the formation of passive films, increases the corrosion potential of stainless steel[5,16–17], and improves the strength of AlCrFeNiMo$_x$ and CoCrFeNiMo$_x$ HEAs due to the formation of σ phase[18–19]. The resultant multi-elemental phase is a solution phase consisting of NiMo, FeMo, Fe-Cr-Mo, Cr-Mo-Ni, and Al-Mo-Ni intermediate phases[6,20–21]. It is demonstrated that the formation of σ phase is directly related to the valence electron concentration (VEC), which is a parameter used to predict σ phase formation in HEAs[22]. Mechanical properties and corrosion resistance are important criteria for the performance evaluation of coatings. However, the corrosion resistance of HEAs containing σ phase is rarely reported. In this research, the effects of Mo content on the microstructure, hardness, and corrosion resistance of AlCoCrFeNiMo$_x$ HEA coatings prepared by laser cladding were investigated.

1 Experiment

The AlCoCrFeNiMo$_x$ HEA coatings were prepared by laser cladding through the Laserline LDF-4350 laser equipment. The Al, Cr, Fe, Ni, Mo, and Co element powders (purity of 99.9wt%) were used as cladding materials. The composition, VEC, and melting point T_m of the coatings are shown in Table

Received date: March 24, 2023
Foundation item: National Natural Science Foundation of China (51774179); Natural Science Foundation of Liaoning Province (20180550546); Joint Fund of State Key Laboratory of Metal Material for Marine Equipment and Application (HGSKL-USTLN(2021)03)
Corresponding author: Zhu Xiaolei, Ph. D., Senior Engineer, Steel Research Institute, Angang Group, Anshan 114009, P. R. China, E-mail: zxlzxl2005@126.com

1. When the Mo content of AlCoCrFeNiMo$_x$ HEAs is 0at%, 9.09at%, 16.67at%, 23.08at%, and 28.57at%, i.e., x=0, 0.5, 1.0, 1.5, 2.0, the corresponding specimens were named as Mo_0, $Mo_{0.5}$, $Mo_{1.0}$, $Mo_{1.5}$, and $Mo_{2.0}$, respectively. Pure iron (99.5wt% purity) was used as the matrix material in this experiment, which could accurately analyze and characterize the structure and properties of HEAs. The size of the pure iron specimen was 170 mm×140 mm×10 mm. The surface of pure iron specimens was polished, cleaned with absolute ethanol, and dried by hairdryer. The as-prepared pure iron specimens were preheated in a vacuum furnace at 100 °C for 24 h. The laser cladding experiments were conducted under argon atmosphere, and a layer of mixed powders with thickness of 1 mm was placed on the specimen. The processing parameters were as follows: laser power of 1350 W, scanning speed of 20 mm/s, and spot diameter of 3 mm. To eliminate the stress, the specimens were annealed at 900 °C for 5 h.

Analyses of X-ray diffraction (XRD), X-ray photoelectron spectroscopy (XPS), and electrochemical performance of specimens were conducted. The specimens were cut by wire electrical discharge machining (WEDM) into the ones with size of 15 mm×5 mm×1 mm. Then, the coating surface was polished by sandpaper to obtain a smooth surface. The structural features of the specimens were examined by XRD system (PANalytical X-pert Power) under the conditions of Cu Kα radiation, 2θ=10°–90°, scanning speed of 4°/min, and step length of 0.065°. The electrochemical performance was measured by an electrochemical workstation (AUTOLAB PGSTAT302N, China) in 3.5wt% NaCl solution with test potential of −1.2–1.2 V and test speed of 1.0 mV/s. A platinum electrode was served as the auxiliary electrode, and a saturated AgCl electrode was served as the reference electrode. XPS system (Escalab 250Xi, USA) with monochromatic Al Kα excitation was used to detect the chemical valence states of metal elements in the film formed on the coating surface of specimens after immersion in 3.5wt% NaCl solution for 120 h. XPS results were analyzed by Avantage software. The specimens were cut by WEDM method into the ones with 5 mm×5 mm×2 mm in size for the scanning electron microscope (SEM) observation, and a conductive metallographic inlay was applied. The specimens were corroded in aqua regia for 5 s after milling and polishing. The cross-section morphology and microstructure of HEA coatings were analyzed by SEM (HITACHI-3400N, Japan) coupled with an energy dispersive spectroscope (EDS, TEAM PEGASUS2040, USA). The hardness was measured by Vickers Hardness Tester (Qness Q10A) with the load of 1000 g for 15 s, and five sets of data were measured every 0.2 mm in distance. Transmission electron microscope (TEM, FEI Talos F200) coupled with EDS (FEI Super X, USA) was used for TEM observation. TEM specimens were thinned into the ones of approximately 30 μm in thickness by SiC paper, and the ion milling was used to obtain the electron-transparency area.

2 Results and Discussion

2.1 Constituent phases and microstructure

Table 1 shows VEC values of AlCoCrFeNiMo$_x$ alloys, which are calculated through Eq.(1), as follows:

$$\mathrm{VEC} = \sum_{i=1}^{n} c_i (\mathrm{VEC})_i \quad (1)$$

where c_i is the atomic percentage of the ith element, $(\mathrm{VEC})_i$ is VEC value of ith element, and n is the number of components. It can be seen that VEC values are between 6.88 and 7.84, which satisfies the σ phase formation conditions[22]. Fig. 1 shows XRD patterns of the AlCoCrFeNiMo$_x$ (x=0.5, 1.0, 1.5, 2.0) coatings. Only bcc and σ phases (Fe-Al-Mo and Mo-Cr-Fe) can be identified in the AlCoCrFeNiMo$_x$ coatings, which is attributed to the high chemical compatibility of the constituent elements and the contribution of high mixing entropy to the phase stability of HEAs[1–2,7]. With increasing the Mo content, the diffraction peaks gradually shift to the left side, indicating the gradual increase in lattice constant. The diffraction peak of the σ phase (Mo-Cr-Fe) is slightly enhanced when x>1.0.

SEM images at secondary-electron (SE) mode of the AlCoCrFeNiMo$_x$ HEA coatings are shown in Fig. 2. The chemical composition of different regions and phases was obtained by EDS, as listed in Table 2. There is an error in the characterization of chemical composition of $Mo_{1.0}$, $Mo_{1.5}$, and $Mo_{2.0}$ specimens due to slight differences in element and phase contents. However, the characterization of Al enrichment can still be clearly identified. The light and dark phases in $Mo_{0.5}$ specimen are indicated by ID and DR, respectively. XRD and EDS results show that the microstructure of $Mo_{0.5}$ specimen is mainly composed of (Al, Ni)-rich bcc phase (ID region) and (Mo-Cr-Fe)-rich σ phase (DR region), as shown in Fig. 2a. With increasing the Mo content to 16.67at%, DR and IR regions have the same phases, as shown in Fig. 2b. However, these two phases are more refined, compared with those in $Mo_{0.5}$ specimen, indicating the microstructure refinement with more Mo addition. The solid solution in AlCoCrFeNiMo$_x$ alloys is no longer the primary phase with further increasing

Table 1 Composition, VEC, and T_m of AlCoCrFeNiMo$_x$ HEAs

HEAs	Al content/at%	Co content/at%	Cr content/at%	Fe content/at%	Ni content/at%	Mo content/at%	VEC	T_m/°C
Mo_0	20	20	20	20	20	0	7.20	1400.7
$Mo_{0.5}$	18.18	18.18	18.18	18.18	18.18	9.09	7.10	1511.5
$Mo_{1.0}$	16.67	16.67	16.67	16.67	16.67	16.67	7.00	1603.9
$Mo_{1.5}$	15.38	15.38	15.38	15.38	15.38	23.08	6.90	1682.1
$Mo_{2.0}$	14.29	14.29	14.29	14.29	14.29	28.57	6.88	1749.1

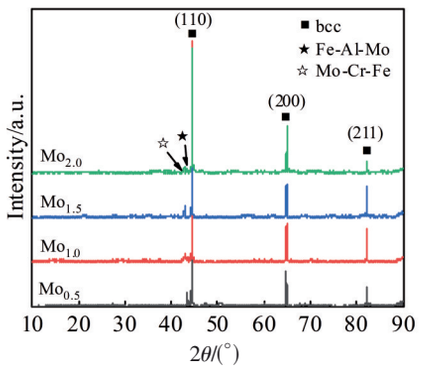

Fig.1 XRD patterns of AlCoCrFeNiMo$_x$ HEA coatings

the Mo content, thereby promoting the Mo-rich phase formation when x>1.0. Fig. 2c shows three characteristic regions in Mo$_{1.5}$ specimen, and they are identified as α, β, and γ regions. Both the amount and the size of the precipitates are increased when Mo content increases to 23.08at%, and a large number of α regions appear in the bcc phase, as indicated in Fig. 2c. According to Fig. 2d, the microstructure of Mo$_{2.0}$ specimen is similar to that of Mo$_{1.5}$ specimen, but the α and β regions grow significantly. Since XRD patterns and SEM images of Mo$_{0.5}$ and Mo$_{1.0}$ specimens are similar, these two specimens are further analyzed by TEM, and the corresponding selected area electron diffraction (SAED) patterns are also shown in Fig. 3. TEM and EDS analysis results show that the α region is the AlN phase, β region is the strip (Fe, Ni)-rich bcc phase, and γ region is a composite phase consisting of (Mo-Cr-Fe)-rich σ phase (γ_1) and fine (Fe, Ni)-rich bcc phase. The theoretical melting point of AlCoCrFeNiMo$_x$ HEAs can be calculated by Eq. (2)[23], as follows:

$$T_{\mathrm{m}} = \sum_{i=1}^{n} c_i (T_{\mathrm{m}})_i \quad (2)$$

where $(T_{\mathrm{m}})_i$ is the melting point of ith element in the alloy. The calculation results are presented in Table 1. It can be seen that the melting point of AlCoCrFeNiMo$_x$ HEAs is increased with increasing the Mo content. Owing to the higher melting point, faster solidification rate of Mo$_{1.5}$ and Mo$_{2.0}$ specimens can prevent the escape of nitrogen from the powder. Thus, the nitrogen atoms in the Al solution are trapped during the solidification process to form the common secondary phase particles (AlN), which have high melting point of 2227 °C, and they usually solidify in the first place. It is reported that the secondary phase particles can easily form in various alloys[24–25]. Since AlN has high melting point and low surface energy, other atoms usually nucleate on the surfaces[26]. Hence, some (Fe, Ni)-rich bcc phases nucleate preferentially around the AlN phase in Mo$_{1.5}$ and Mo$_{2.0}$ specimens, and they gradually grow into strip bcc structures during solidification. Therefore, bcc and σ phases nucleate on the AlN phase, forming a fine phase structure. The iron content in the coating is higher than its theoretical value, which can be attributed to the diffusion of iron atoms from matrix to coating. This phenomenon is inevitable in the manufacture process and it is also the main difference between HEA coatings and as-cast HEAs.

2.2 Hardness

Fig.4 shows the hardness of different AlCoCrFeNiMo$_x$ HEA coatings. The average hardness (HV$_1$) of the cladding layer of Mo$_{0.5}$, Mo$_{1.0}$, Mo$_{1.5}$, and Mo$_{2.0}$ specimens is 6154.4, 9819.6, 9966.6, and 10652.6 MPa, respectively, indicating that the coating hardness is gradually improved with increasing the Mo content. When x=0.5 and x=1.0, the microstructure is refined and a large number of grain boundaries appear, therefore hindering the dislocation movement. With further increasing the Mo content to 23.08at% and 28.57at%, the

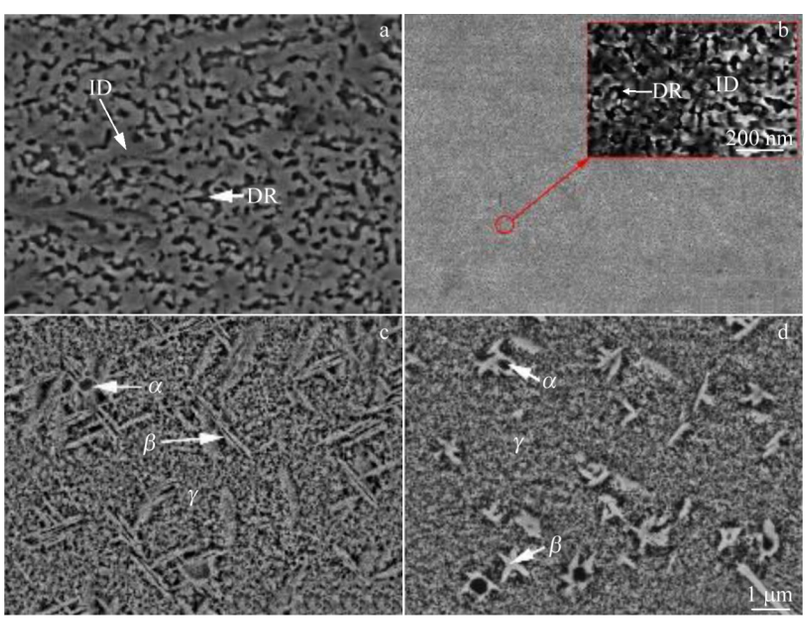

Fig.2 SEM microstructures of different AlCoCrFeNiMo$_x$ HEA coatings: (a) Mo$_{0.5}$ specimen; (b) Mo$_{1.0}$ specimen; (c) Mo$_{1.5}$ specimen; (d) Mo$_{2.0}$ specimen

Table 2 Composition of different regions in AlCoCrFeNiMo$_x$ HEA coatings (at%)

Specimen	Region and phase	Al	Co	Cr	Fe	Ni	Mo
Mo$_{0.5}$	DR	8.89	7.28	15.23	42.59	3.42	22.59
	ID	13.75	14.99	14.60	30.99	16.14	9.52
Mo$_{1.0}$	All regions	12.27	11.72	12.83	40.60	11.94	10.64
Mo$_{1.5}$	α	20.29	5.93	13.70	32.83	2.71	24.53
	β	0	7.72	17.95	41.51	3.15	29.66
	γ	0	7.37	17.24	42.61	3.35	29.43
Mo$_{2.0}$	α	24.56	5.35	8.93	33.24	3.72	24.20
	β	1.28	7.14	11.73	44.96	4.18	30.71
	γ	1.37	7.28	11.04	44.29	4.55	31.47

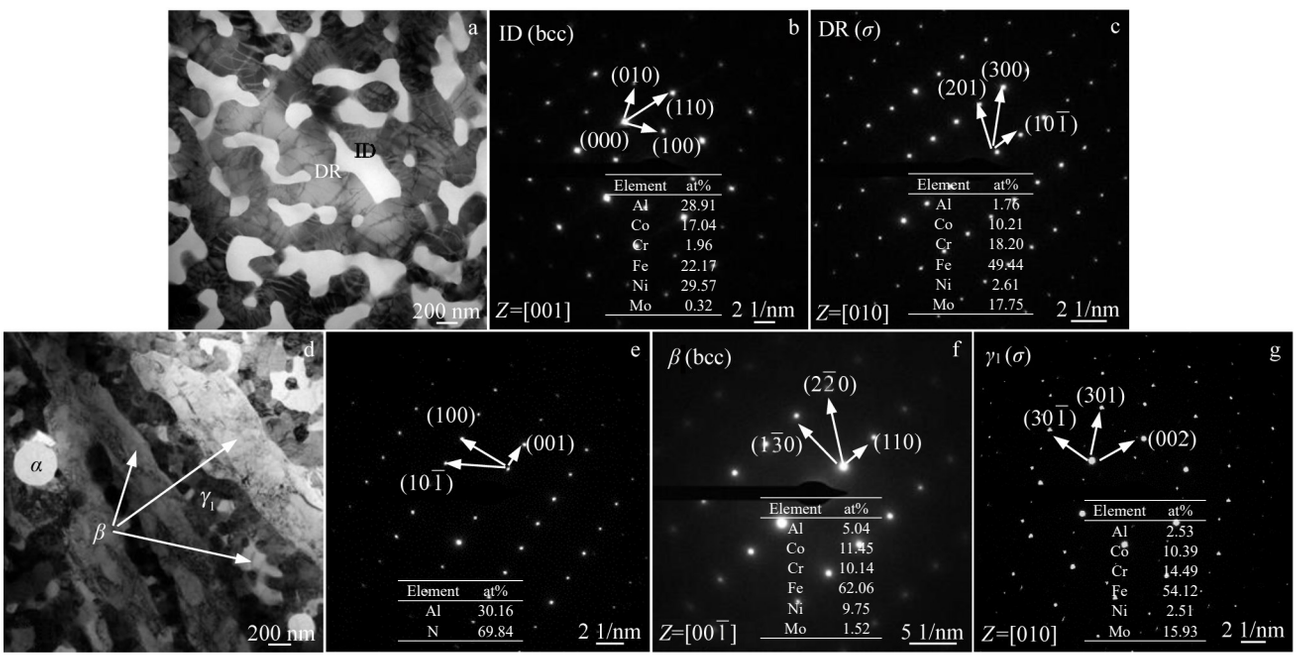

Fig.3 TEM images (a, d) and corresponding SAED patterns (b–c, e–g) of Mo$_{1.0}$ specimen (a–c) and Mo$_{1.5}$ specimen (d–g)

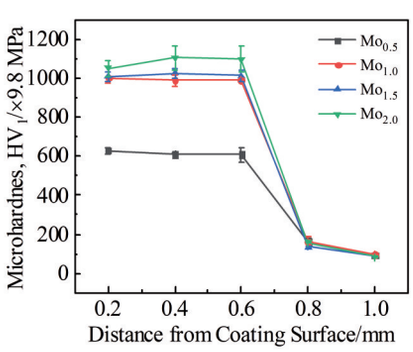

Fig.4 Hardness of AlCoCrFeNiMo$_x$ HEA coatings

hardness is still increased but with a small increment. This is because growth of (Fe, Ni) -rich bcc phases is normally associated with the AlN phase, resulting in coarse structure and less grain boundaries, and thereby reducing the dislocation blocking effect. The coating hardness is less uniform when x>1.5.

2.3 Corrosion resistance

The potentiodynamic polarization curves of AlCoCrFeNiMo$_x$ HEA coatings in 3.5wt% NaCl solution are shown in Fig. 5. The self-corrosive potential (E_{corr}) and self-corrosive current density (I_{corr}) of the alloys can be obtained by Tafel linear extrapolation, as listed in Table 3. The self-corrosive current density is firstly decreased and then increased with increasing the Mo content. When x=0.5 and x=1.0, the microstructure refinement promotes the uniform element distribution and reduces the local potential difference, therefore enhancing the corrosion resistance. With increasing the Mo content, the AlN phase precipitates appear in the cladding layer and the local potential difference is increased, thus reducing the corrosion resistance. The Mo$_{1.0}$ specimen has the smallest self-corrosive current density, I_{corr}=1.355 μA·cm^{-2} (at E_{corr}=0.357 V), presenting the optimal corrosion resistance. The corrosion resistance is closely associated with the oxide film on the coating surface, which efficiently inhibits the penetration of electrolytes into the coating and reduces the dissolution rate.

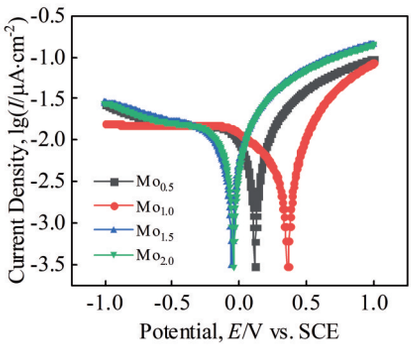

Fig.5 Potentiodynamic polarization curves of $AlCoCrFeNiMo_x$ HEA coatings in 3.5wt% NaCl solution

Table 3 Self-corrosive potentials (E_{corr}) and self-corrosive current densities (I_{corr}) of $AlCoCrFeNiMo_x$ HEA coatings in 3.5wt% NaCl solution

Specimen	Self-corrosive potential, E_{corr}/V	Self-corrosive current density, I_{corr}/μA·cm^{-2}
$Mo_{0.5}$	0.114	2.250
$Mo_{1.0}$	0.357	1.355
$Mo_{1.5}$	−0.052	1.979
$Mo_{2.0}$	−0.042	2.288

The passive film formed on the $Mo_{1.0}$ specimen coating in 3.5wt% NaCl solution was analyzed by XPS, and the results are shown in Fig. 6. It can be seen that the passive film consists of Ni, Co, Fe, Al, Cr, Mo, and O, indicating that the passive film consists of the oxides of these metal elements. Fig.6b and 6d show that Al and Cr primarily exist in the form of Al_2O_3 and Cr_2O_3. The Co 2p peak is located at the binding energy of 781.3 and 787.6 eV, as shown in Fig.6c, suggesting that Co exists in the form of CoO. Fe exists in the forms of FeO and Fe_2O_3, according to Fig. 6e. Two strong peaks of MoO_3 at 235.6 and 232.4 eV can be clearly observed in Fig.6f. According to Fig.6g, NiO exists in the alloy.

Several dissolution reactions of the oxides may occur during the treatment process, as follows:

$$Al_2O_3+6Cl^-=2AlCl_3+3O^{2-} \quad (3)$$

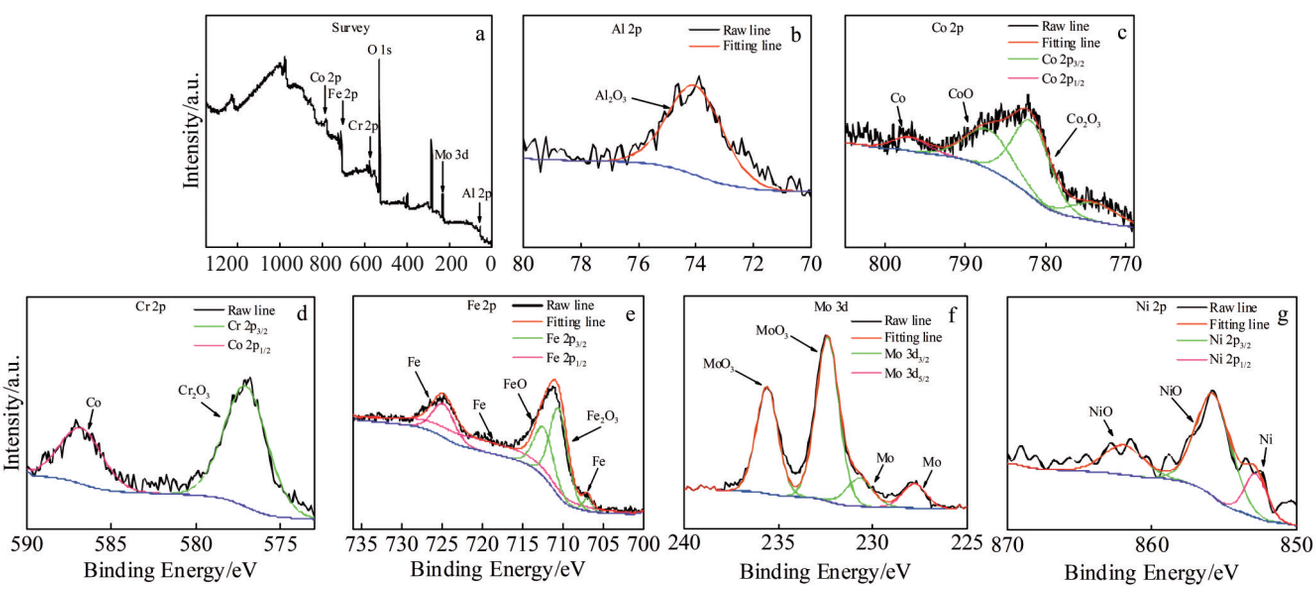

Fig.6 XPS results of passive film on $Mo_{1.0}$ coating surface: (a) overall; (b) Al 2p; (c) Co 2p; (d) Cr 2p; (e) Fe 2p; (f) Mo 3d; (g) Ni 2p

$$CoO+2Cl^-=CoCl_2+O^{2-} \quad (4)$$

$$Cr_2O_3+6Cl^-=2CrCl_3+3O^{2-} \quad (5)$$

$$FeO+2Cl^-=2FeCl_2+O^{2-} \quad (6)$$

$$Fe_2O_3+6Cl^-=2FeCl_3+3O^{2-} \quad (7)$$

$$MoO_3+6Cl^-=MoCl_3+3O^{2-} \quad (8)$$

$$NiO+2Cl^-=NiCl_2+O^{2-} \quad (9)$$

Fig. 7 shows the standard Gibbs free energy ΔG^{θ} of the abovementioned reactions with increasing the temperature, which is calculated by HSC Chemistry 9.0 software. The main failure of the passive film is caused by the replacement of oxygen by soluble Cl^- ions. Thermodynamic calculation results show that all reactions are non-spontaneous at room temperature, indicating that the passive film effectively resists the Cl^-

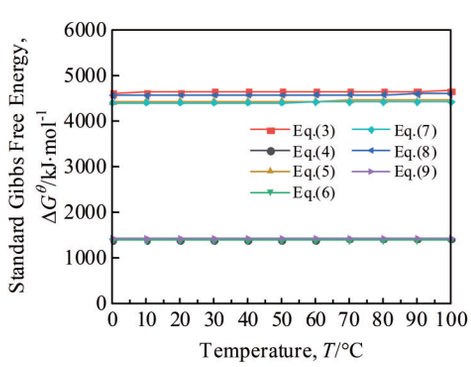

Fig.7 Standard Gibbs free energies of different dissolution reactions of $AlCoCrFeNiMo_x$ HEA coatings

ion erosion and protects the coating matrix in a neutral solution. The ΔG^{θ} values of Eq. (3), Eq. (5), and Eq. (8) are higher than those of other reactions, inferring that Al_2O_3, MoO_3, and Cr_2O_3 in the passive film have better resistance against the Cl^- ion erosion in the neutral solution. Additionally, the iron oxide does not participate in the corrosion protection owing to its loose structure.

3 Conclusions

1) The microstructure of $AlCoCrFeNiMo_x$ high entropy alloy (HEA) coating is changed from the (Al, Ni)-rich body-centered cubic (bcc) phase+(Mo-Cr-Fe)-rich σ phase into the (Fe, Ni)-rich bcc phase+(Mo-Cr-Fe)-rich σ phase+(Al-Fe-Mo)-rich σ phase+a little AlN with increasing the Mo content.

2) The hardness of $AlCoCrFeNiMo_x$ HEA coating is gradually increased with increasing the Mo addition. Excess Mo addition results in the brittle coatings. The optimal hardness (HV_1) of $AlCoCrFeNiMo_x$ HEA coating is 9819.6 MPa when x=1.0.

3) The self-corrosion potential of the $AlCoCrFeNiMo_x$ HEA coating is increased with increasing the Mo addition. The $AlCoCrFeNiMo_{1.0}$ coating with corrosion potential E_{corr}=0.357 V and corrosion current density I_{corr}=1.355 μA·cm^{-2} shows the optimal corrosion resistance in 3.5wt% NaCl solution.

References

1 Yeh J W, Chen S K, Lin S J *et al*. *Advanced Engineering Materials*[J], 2004, 6(5): 299
2 Senkov O N, Wilks G B, Miracle D B *et al*. *Intermetallics*[J], 2010, 18(9): 1758
3 Li X C, Dou D, Zheng Z Y *et al*. *Journal of Materials Engineering and Performance*[J], 2016, 25(6): 2164
4 Jiang L, Cao Z Q, Jie J C *et al*. *Journal of Alloys and Compounds*[J], 2015, 649: 585
5 Tian H C, Cheng X Q, Wang Y *et al*. *Electrochimica Acta*[J], 2018, 267: 255
6 Wu W, Jiang L, Jiang H *et al*. *Journal of Thermal Spray Technology*[J], 2015, 24(7): 1333
7 Li K Y, Liang J, Zhou J S. *Surface and Coatings Technology*[J], 2022, 449: 128 978
8 Liu H, Gao Q, Hao J B *et al*. *Rare Metal Materials and Engineering*[J], 2022, 51(6): 2199
9 Kao Y F, Chen S K, Chen T J *et al*. *Journal of Alloys and Compounds*[J], 2011, 509(5): 1607
10 Butler T M, Weaver M L. *Journal of Alloys and Compounds*[J], 2017, 691: 119
11 Li X F, Feng Y H, Wang X *et al*. *Journal of Alloys and Compounds*[J], 2022, 926: 166 778
12 Wang W R, Wang W L, Yen J W. *Journal of Alloys and Compounds*[J], 2014, 589: 143
13 Zhang C, Zhang F, Diao H Y *et al*. *Materials & Design*[J], 2016, 109: 425
14 Ma X F, Sun Y N, Cheng W J *et al*. *Journal of Central South University*[J], 2022, 29(10): 3436
15 Zhou Z J, Jiang F L, Yang F Z *et al*. *Materials Letters*[J], 2023, 335: 133 714
16 An L C, Cao J, Wu L C *et al*. *Journal of Iron & Steel Research International*[J], 2016, 23(12): 1333
17 Saidi D, Zaid B, Souami N *et al*. *Journal of Alloys and Compounds*[J], 2015, 645: 45
18 Dong Y, Lu Y P, Kong J R *et al*. *Journal of Alloys and Compounds*[J], 2013, 573: 96
19 Shun T T, Chang L Y, Shiu M H. *Materials Science and Engineering A*[J], 2012, 556: 170
20 Hsu C Y, Wang W R, Tang W Y *et al*. *Advanced Engineering Materials*[J], 2010, 12(1–2): 44
21 Praveen S, Murty B S, Kottada R S. *Journal of Nanoscience and Nanotechnology*[J], 2014, 14(10): 8106
22 Tsai M H, Tsai K Y, Tsai C W *et al*. *Materials Research Letters*[J], 2013, 1(4): 207
23 Yang X, Zhang Y. *Materials Chemistry and Physics*[J], 2012, 132(2–3): 233
24 Martinavicius A, Van Landeghem H P, Danoix R *et al*. *Materials Letters*[J], 2017, 189: 25
25 Shelton R K, Dunand D C. *MRS Online Proceedings Library*[J], 1995, 398(1): 457
26 Liang T, Zhang B, Sun Y X *et al*. *Materials Today Communications*[J], 2023, 34: 105 277

Mo元素对激光熔覆$AlCoCrFeNiMo_x$高熵合金涂层组织性能的影响

沙明红[1,2]，王　爽[2,3]，李胜利[1]，贾春堂[2,3]，黄天荡[1]，朱晓雷[2,3]，艾新港[1]，廖湘巍[2,3]

(1. 辽宁科技大学 材料与冶金学院，辽宁 鞍山 114051)

(2. 海洋装备用金属材料及其应用国家重点实验室，辽宁 鞍山 114009)

(3. 鞍钢集团 钢铁研究院，辽宁 鞍山 114009)

摘　要：采用激光熔覆的方法制备$AlCoCrFeNiMo_x$高熵合金涂层。研究Mo元素含量对涂层微观结构、硬度及耐腐蚀性的影响。结果表明，随着Mo含量的增加，微观组织从富(Al, Ni)的体心立方（bcc）相和富(Mo-Cr-Fe)的σ相，转变为富(Fe, Ni)的bcc相、富(Mo-Cr-Fe)的σ相、富(Al-Fe-Mo)的σ相与少量AlN相。此外，涂层的显微硬度（HV_1）从6154.4 MPa增加到10652.6 MPa。随着Mo含量的添加，涂层在3.5%（质量分数）氯化钠溶液中的自腐蚀电位升高，当Mo含量为x=1.0时，涂层的耐腐蚀性能最好。

关键词：高熵合金；激光熔覆；耐腐蚀性能；硬度；微观组织

作者简介：沙明红，女，1976年生，博士，副教授，辽宁科技大学材料与冶金学院，辽宁 鞍山 114051，电话：0412-5929535，E-mail：320003200040@ustl.edu.cn